GEOPHYSICAL CASE HISTORY OF NORTH SILVER BELL, PIMA CO., ARIZONA: A SUPERGENE-ENRICHED PORPHYRY COPPER DEPOSIT

Mark W. Thoman, Regional Geologist, Minera Phelps Dodge Mexico, Tucson, Az
Kenneth L. Zonge, President, Zonge Engineering and Research Organization, Tucson, Az
Dexin Liu, Geophysicist, Zonge Engineering and Research Organization, Tucson, Az

INTRODUCTION AND SUMMARY

The Silver Bell district is within the porphyry-copper province of southwestern North America (Figure 1), located 35 miles northwest of Tucson, Arizona on the south side of the Silver Bell Mountains. Mineralization in the district consists of at least three distinct disseminated porphyry copper deposits and several skarn replacement deposits. Disseminated primary and supergene-enriched porphyry copper mineralization were mined in two open pits, El Tiro and Oxide, by ASARCO, mainly during the period 1954-1977. Total production for that period is reported at 75.66 million tonnes (Mt) at 0.80% copper (Graybeal, 1982). The North Silver Bell deposit is located at the north end of the district and represents a leachable resource of in excess of 80 Mt at an average grade of 0.40% copper contained mostly within an enrichment blanket of chalcocite. When the geophysical work was being done, in 1993-1994 and again in 1996, the deposit was not being mined. Mining of North Silver Bell by ASARCO began in 1997.

In early 1993, the area was suggested by J. M. Guilbert of the University of Arizona as a good site for a baseline geophysical study over a porphyry copper deposit. The deposit was well defined by drilling and surface mapping and did not have any significant surface disturbance or excessive cultural contamination such as numerous powerlines and fences. The approach was to survey the area with a variety of geophysical techniques and develop a comprehensive geophysical signature of the deposit that would have relevance to exploration for porphyry copper deposits elsewhere. ASARCO was essential to the project by allowing access to the deposit and making available company information regarding the deposit. The study was used as the basis for a master's thesis at the University of Arizona by K. C. Foreman (1994).

Geophysical surveys conducted over the deposit by Zonge Engineering and Research Organization (ZERO) personnel included: ground magnetics, dipole-dipole complex resistivity (CR), reconnaissance induced polarization (RIP), controlled source audio-frequency magneto-tellurics (CSAMT) and transient electromagnetics (TEM and NanoTEM). Additional data include CR rock measurements on core specimens from drill holes within the deposit and airborne magnetics and EM flown by World Geoscience in 1993. Except for the airborne data from World Geoscience, all data were processed at ZERO's office in Tucson, Arizona. TEM, IP and CSAMT data were modeled with proprietary smooth-model inversions.

The magnetic signature of the deposit is a low within a regional magnetic high. At the scale of the deposit, ground magnetics distinguishes the alteration zoning, with weak local highs in the potassic zone, lower responses in the phyllic zone and higher increasing values in the propylitic zone. Sulfide mineralization, mostly pyrite with lesser chalcopyrite and chalcocite, is characterized by moderate to high induced polarization (30-60 milliradians). The strongest IP response is correlated with quartz-sericite-pyrite in the phyllic alteration zone. The chalcocite mineralization has an anomalous, but lower, IP response that is partially masked by the laterally adjacent or underlying stronger pyrite response. Decoupled CR or spectral IP responses from the field survey when compared with those obtained for laboratory rock measurements indicate different type responses for pyrite as compared to those for mixed sulfides such as chalcocite-pyrite and pyrite-chalcopyrite. These differences in spectral responses may reflect a combination of changes in grain sizes as well as sulfide species.

Anomalous RIP responses define the area hosting mineralization, including the pyritic halo. The magnitudes of the RIP responses are lower than those obtained from the dipole-dipole survey as would be expected when considering the contributive volumetric effects of a RIP measurement as compared to a dipole-dipole one. Smooth models of apparent resistivity from the CSAMT survey allow for lateral discrimination of alteration zoning, with the lowest resistivities centered on the phyllic and strong phyllic alteration. Vertically, a lower resistivity layer on at least one CSAMT line approximately coincides with the enrichment zone. Laterally across the CSAMT lines, breaks in resistivities relate to faults and changes in lithology, including passing from outcrop to alluvium.

GEOLOGY OF THE SILVER BELL DISTRICT AND THE NORTH SILVER BELL DEPOSIT

The geology of the Silver Bell district has been described in numerous works. One of the best overviews is the article by F. T. Graybeal (1982) on the El Tiro area in the volume "Advances in the Geology of the Porphyry Copper Deposits, Southwestern North America". This article, an earlier article by Richard and Courtright (1966) on the Silver Bell district in "Geology of Porphyry Copper Deposits, Southwestern North America" and various master's theses provide the content for this description of the district and deposit geology.

ROCK UNITS

A simplified geologic map of the district (Figure 2) is excerpted from a master's thesis by Kanbergs (1980). The oldest units consist of thermally metamorphosed and hydrothermally altered sedimentary units including quartzite and re-crystallized limestones (marbles). Suggested correlation of the units is with the Paleozoic Bolsa and Abrigo formations exposed in the Waterman Mountains immediately to the south, but intense alteration and faulting do not allow for conclusive identification of the units. These units are exposed along a northwest trend and are host to skarn mineralization that was the original mining interest of the district. To the southwest, the Paleozoic sedimentary units are engulfed by an alaskite intrusion of interpreted Mesozoic age. Older Mesozoic units include clastic units exposed in the southwest part of the district.

Northeast of the trend of Paleozoic units is a widespread dacite porphyry that is interpreted as a sill-like body. The dacite porphyry is estimated to be as much as 3,400 ft thick near the El Tiro pit, with thinning to the northeast. In addition to the main mass of dacite porphyry, dikes of this unit cut Mesozoic clastic rocks and are cut by quartz monzonite porphyry. The dacite porphyry may be compositionally more of a latite. In places, the dacite porphyry hosts some lower-grade supergene mineralization.

On Kanberg's map, Cretaceous volcanic and volcaniclastic units include the Claflin Ranch Formation, the Silver Bell complex and the Mount Lord ignimbrite. These units are not mentioned by Graybeal (1982), but are briefly described in an earlier description of the district by Richard and Courtright (1966). These volcanic units preceded or were contemporaneous with the intrusion of the porphyry suite that introduced the copper mineralization. The suite is dominantly quartz monzonite in composition. An early phase in the suite was a series of syenodiorite porphyry dikes. Another phase was the quartz monzonite stocks that were centers for mineralization. Other phases included monzonite porphyry dikes, granodioritic dikes and both intrusion and intrusive breccias. Intrusive breccias and pebble dikes have a strong component of fluidization and entrainment of rock clasts. Intrusion breccias are found near the contacts of the quartz-monzonite stocks. Besides Quaternary alluvium, the youngest units in the district are some mid-Tertiary andesitic and latitic dikes and consolidated caliche-cemented conglomerate equivalent to the Gila Conglomerate.

STRUCTURAL GEOLOGY

Regionally, the Silver Bell district is along the major northwest-trending the Silver Bell-Bisbee discontinuity that along with the parallel Comobabi-Nogales discontinuity and the Sawmill fault defines distinctive Paleozoic and Mesozoic rock assemblages in southern Arizona (Titley, 1982). In the Silver Bell district, Richard and Courtright (1966) inferred a major west-northwest fault or series of faults that partially controlled the emplacement of the porphyry suites with their attendant mineralization and alteration. This west-northwest trending zone of alteration and mineralization extends from the Oxide pit on the east to the El Tiro pit on the west. At the El Tiro area, the trend of mineralization and alteration changes from a north-northwest to north orientation. This change in orientation reflects the presence of two or more major northwest to north-northwest faults that controlled the intrusion of the porphyry suite.

The N40°W El Tiro fault is interpreted as the original contact between the Mesozoic clastic units to the southwest and the Paleozoic units to the northeast. This major structure may have controlled the emplacement of the alaskite, the dacite porphyry and some of the quartz monzonite stocks with their mineralization and alteration.

A second structure oriented N05°W may be a splay off of the El Tiro fault. This interpreted fault parallels the elongation of the Daisy and El Tiro stocks as well as the alignment of these two stocks and the North Silver Bell stock. To the west of this inferred fault is the north-northeast to north-northwest striking postmineral Atlas fault. This structure brings Gila Conglomerate to the west in contact with older units to the east.

Numerous northeast to east-northeast to west-northwest monzonite porphyry dikes are mapped in the district, principally to the east and northeast of the El Tiro and North Silver Bell areas. It is interpreted that these dikes intruded premineral structural elements that intersect the northwest El Tiro fault at the present location of the El Tiro pit. This structural intersection is interpreted by some to have localized the porphyry mineralization in that locality. Another suggested interpretation (Heidrick, 1974) is that the northeast orientations reflect hydraulic fracturing during emplacement of water-saturated magmas.

Richard and Courtright's (1966) map shows orientations of mineralized fissures or fractures within the zone of alteration and disseminated pyrite. Orientations of mineralized fractures changes from dominantly north-northeast at the Oxide pit to east-northeast at the El Tiro pit. According to Graybeal (1982), mineralization is both disseminated and along fractures. Fractures host most of the mineralization away from the potassic zone. In the phyllic alteration, most of the mineralization is along fractures. These zones have the highest total sulfide content (5-7%) which is dominantly pyrite.

MINERALIZATION AND ALTERATION

Mineralization in the Silver Bell district consists principally of disseminated copper sulfides. Initial mining in the period from 1865 to 1930 exploited high-grade skarn zones within blocks of metamorphosed Paleozoic units. The exploited skarn mineralization was dominantly chalcopyrite (average grade of 3.5%) with high silver values in some bodies. Lesser amounts of sphalerite are present in places. Part of the thermal metamorphism of the Paleozoic and Mesozoic units may be related to the intrusion of the alaskite and dacite porphyry. Skarn formation related to the intrusion of quartz monzonite produced veins and replacements with pyrite and chalcopyrite, silicate skarn minerals, principally garnet, and marble. Magnetite is present in places, as are minor amounts of pyrrhotite. Timing of the skarn formation and mineralization with respect to the other alteration-mineralization types at Silver Bell is not well established, but is believed to have been relatively early, possibly synchronous with potassic and propylitic alterations.

Most of the disseminated chalcopyrite mineralization was introduced during the emplacement of the quartz monzonite stocks along with the development of potassic alteration. Simplistically, potassic alteration consisted of early-formed veinlets of biotite with chalcopyrite and pyrite and later K-feldspar as vein material and as selvages, some of which is associated with molybdenite mineralization. A weak pervasive sericite alteration is present within the potassic zones. Degree and intensity of potassic alteration is somewhat dependent on host lithology, with the dacite and quartz monzonite showing more developed and pervasive alteration than the alaskite. Pyrite to chalcopyrite ratios are lowest within the potassic alteration zones and ratios of disseminated to vein sulfides are highest. Total volume percent sulfides in the potassic zone is 2% at most.

Propylitic alteration is peripheral to potassic alteration zones and characterized by the presence of one or more of the following minerals: epidote, chlorite, calcite, albite and pyrite. This alteration is believed to have formed during the later stages of the potassic alteration. The propylitic alteration is much better developed in the dacite porphyry than in the alaskite. Epidote is the best indicator of the propylitic alteration zone's extent. The weaker development of both potassic and propylitic alteration in the alaskite to the southwest and west gives an apparent asymmetric pattern to the alteration zoning. Pyrite is mostly on joints in the propylitic alteration and total sulfides reach 2-3% by volume but diminish with distance away from the potassic-propylitic contact.

Phyllic alteration is composed of quartz, sericite and pyrite. Phyllic alteration formed after potassic and propylitic alterations and overprints them. At Silver Bell, almost all phyllic alteration is vein controlled. Veins within the phyllic zone are generally much wider than in the potassic zone, so despite the lesser abundance of phyllic veins, there are as much, if not more, total sulfides in the phyllic zone as compared to the potassic zone. Volume percents of sulfides reach 5-7% in the phyllic zone as compared to the 2% observed in the potassic zone. The dominant trend of veins in the phyllic zone, as in the potassic zone, is to the northeast. Unlike the potassic and propylitic alteration types, near the El Tiro area, the phyllic alteration was best developed in the alaskite.

The phyllic alteration on the west side of the El Tiro deposit is believed to have been essential to the formation of the economic supergene chalcocite blanket mined there (Graybeal, 1982). Without the superposing of strong phyllic alteration on potassic alteration there would not have been enough pyrite to generate sufficient sulfuric acid to leach the primary copper mineralization. Graybeal states the lack of strong phyllic alteration at North Silver Bell as the reason why the chalcocite blanket there is much thinner and more irregular than the one at El Tiro.

NORTH SILVER BELL DEPOSIT

The map of deposit geology for North Silver Bell (Figure 3) is taken from a portion of the map given in Graybeal's (1982) article. Volumetrically, the dacite porphyry is the most significant unit. Simplified geology along cross sections is displayed for each of the three complex-resistivity lines. The deposit consists of dacite porphyry intruded by quartz monzonite porphyry. Mineable and leachable chalcocite mineralization consists of 2-3 times supergene enrichment of primary copper grades of 0.10-0.20%. A master's thesis by Piekenbrock (1983) shows a different distribution of the alteration types than what was shown by Graybeal. The alteration zoning from Piekenbrock is shown on Figure 4. As will be shown in discussions of the ground magnetic response and CSAMT resistivities, geophysical data support the interpretation of alteration zoning shown by Piekenbrock. Whereas Graybeal has only one very restricted zone of phyllic alteration to the east of the North Silver Bell stock, Piekenbrock's map has a fairly continuous 1000-1500 ft wide zone of phyllic alteration both north and east of the outcrops of the main stock. Within the phyllic zone, Piekenbrock further differentiates three subzones with increasing intensities of alteration.

In Graybeal's article, the chalcocite enrichment blanket at North Silver Bell is considered poorly developed. Additional drilling and changes in economic factors make the deposit much more favorable than it was originally thought. Whereas the enrichment zone is thinner and of lower average grade than what was mined at El Tiro, the chalcocite mineralization at North Silver Bell represents an equivalent number of tonnes of ore as what was mined in the Oxide and El Tiro combined. Average thickness of the zone is 100 ft with an average grade 0.40% copper. Projection of the chalcocite zone to the surface, along with the proposed pit outline, is shown in Figure 5.

GEOPHYSICAL RESPONSES

Geophysics, principally induced polarization (IP) and magnetics, has been an integral part of exploration for porphyry copper deposits for more than 30 years. With the development of IP equipment and methodology after World War II, IP surveys have become a regularly utilized tool in the search for disseminated sulfide bodies associated with porphyry copper systems. Other geophysical methods used for direct detection of porphyry-copper deposits have been radiometrics and spontaneous or self-potential (SP). Other tools such as various electromagnetic techniques and gravity have had application to specific objectives such as determination of depths to bedrock in covered areas and detection of skarn and/or massive sulfide mineralization associated with porphyry systems.

With IP measurements in the 1970's many researchers investigated the possibility of distinguishing the response of different sulfide species, clays and graphite. Most of this work was done in the frequency domain under such names as spectral IP or complex resistivity. Some investigators concluded that changes in maximum IP response with frequency were solely due to differences in grain sizes, whereas others, while admitting the influence of grain size, believed that changes in peak responses with frequency were related to different mineral species or combinations of species. Despite the lack of universal agreement, there are numerous good studies in the literature.

Generalized geophysical signatures of porphyry copper deposits have included the following listing:

1. magnetic response – regionally, often a low re-entrant within a regional magnetic high; the low is caused by magnetite destructive hydrothermal alteration in the potassic and phyllic zones; at depth within potassic zones, can have magnetite-pyrite veinlets that may impart local higher magnetic response; if porphyry system intruded into carbonates, can get skarns with magnetite; also, magnetics very good for showing regional to district scale structures.

2. IP response – usually moderate to high depending on depth to sulfides; usually have 2% by volume or more total sulfides; variations in response from lower total sulfides in the potassic zone as contrasted with the phyllic zone; other variations in response from deposit to deposit depending on whether 'low' or 'high' sulfide type system; nature of sulfide mineralization, whether on fractures or disseminated; effects of clays on magnitude of responses; effect of mixtures of sulfide species.

3. lower resistivities – due to the strongly fractured nature of porphyry systems, particularly in phyllic zones, along with interconnected sulfide veinlets; leached capping with copper-oxide mineralization can often be reflected in higher resistivities than underlying or adjacent chalcocite enrichment or primary mineralization.

4. spontaneous or self potential – not utilized as much in earlier exploration; strong anomalies as much as 500 millivolts such as documented over the Lone Star porphyry deposit in the Safford district (Robinson and Cook, 1966); chemical reactions at redox boundaries (water table) within sulfide mineralization generating battery-like effects; effects may be more pronounced in pyritic zones (phyllic).

5. radiometrics – principally radiometric potassium response from secondary biotite, K-spar and sericite in potassic and phyllic alteration; in some instances, plots of anomalous potassium (Ka) rather than just radiometric potassium better for discriminating porphyry copper, particularly where porphyry copper within a biotite granodiorite batholith.

For this case history, efforts were concentrated more on electrical and electromagnetic methods that focused on IP responses and resistivities associated with changes in sulfide mineralization and alteration. In addition to the traditional geophysical approach to porphyry exploration using magnetics and IP, electromagnetic methods, CSAMT and TEM, were utilized to test their efficacy in mapping resistivity (conductivity) contrasts associated with mineralization and alteration. Also, the reconnaissance IP (RIP) technique pioneered by Kennecott was used for comparison with the response from the dipole-dipole lines. Figure 6 shows the positioning of the RIP survey points with respect to the area of detailed surveying including CR, magnetic and CSAMT coverage. Figure 7 is a larger scale version of the detailed study area.

MAGNETICS

REGIONAL SCALE

On the residual aeromagnetic map of Arizona (Figure 8), the Silver Bell district occurs along a regional northwest-trending magnetic high (Sumner, 1985). However, some of the porphyry copper deposits of Arizona, e. g. Morenci, Twin Buttes and Mineral Park, are related to arcuate magnetic lows. These lows are interpreted to reflect deep fracture systems where hydrothermal fluids of porphyry systems have destroyed magnetite. At the elevations at which the magnetic data were gathered for the state magnetic map, longer-wavelength anomalies from deeper sources are being sensed. Sumner states that what is being sensed are the plumbing systems to the porphyry systems and not the porphyries themselves.

At the deposit scale, magnetite-destructive alteration at the near surface may be masked or undetected in more regional, higher-elevation surveys. Also, if plumbing systems to the porphyries are being detected in higher-elevation surveys, the magnetite-destructive hydrothermal alteration at depth must be fairly extensive to generate a regional scale low. Whereas this may be the case with the larger porphyry systems such as Morenci, deep-rooted magnetite destruction may not be distinguishable in smaller systems such as Silver Bell. Another consideration is the apparent susceptibilities of the covering and surrounding host rocks to the porphyry deposits.

DISTRICT SCALE

District scale magnetic coverage is provided by east-west flight lines spaced every 200 meters (656 ft) at a draped elevation of 80 meters (262 ft) flown by World Geoscience in 1994. Data are presented on a shaded total magnetic intensity plot (Figure 9). The illumination for the plot is from the northeast to accentuate the dominant northwest structural fabric. The porphyry deposits Oxide, El Tiro and North Silver Bell (NSB) have been approximately located on the plot as have the Atlas fault and two other controlling structures discussed in the geologic portion of this presentation.

The El Tiro and North Silver Bell deposits occur within a low re-entrant within a relatively strong magnetic high. The Oxide deposit occurs along a west-northwest trending magnetic trough that is bounded by magnetic highs. This is the possible west-northwest fault that controlled alteration and mineralization between the Oxide and El Tiro zones. The postmineral northwest-striking Atlas fault is well defined in the magnetic data. The interpreted N05°W structure that controls the elongation of the El Tiro and Daisy stocks as well as aligning them with the North Silver Bell stock is inferred on the magnetic plot. This inferred structure is not as distinct as the northwest-striking faults and could possibly be enhanced by illuminating the data from the west.

Despite the fact that on the regional magnetic data the Silver Bell district does not show as a magnetic low, on this district scale survey, the mineralized area correlates with a fairly subtle low re-entrant zone. There are pronounced magnetic lows on this district plot, some of which correlate with alluvium-covered areas.

DEPOSIT SCALE

Ground magnetic data at North Silver Bell were acquired along 13 lines spaced 400 ft apart. Magnetic readings were taken every 100 ft along the lines for 51,200 ft of coverage. The surveyed grid area falls within the low re-entrant zone noted on the airborne district survey. Two Geometrics 856A proton-precession magnetometers were used; one as the mobile field unit and the other as a base station for recording diurnal variations every three minutes. After correcting

data for diurnal variations, the data were processed using GeoSoft's MAGMAP software. The reduced-to-pole total intensity is shown (Figure 10) with the boundaries for the alteration zones superimposed.

It is readily apparent that there is a fair coincidence with magnetic breaks and the changes in alteration. The changes in magnetic response can not be ascribed to changes in rock type as only two units are present, the quartz monzonite porphyry and the larger mass of dacite porphyry. The propylitic zone has a higher magnetic response, as this type of alteration is not magnetite destructive. Phyllic alteration is developed in zones of most intense fracturing and fluid flow generally resulting in magnetite destruction. In this survey the magnetic response is mixed with an increasing gradient towards the boundary with propylitic alteration. The potassic zone varies from lower magnetic response to localized highs. These localized highs are interpreted as zones with magnetite veining at depth. The deeper portions of root zones of the potassic alteration often have magnetite or magnetite-pyrite veining.

IP RESPONSE

Although dipole-dipole IP data were acquired in the complex-resistivity (CR) mode, a discussion of the spectral character of the responses will be postponed to a later section. The general polarization response obtained over North Silver Bell is similar in magnitude and character to that obtained over other exposed or shallowly buried porphyry systems elsewhere. The results of the reconnaissance (or vector) IP (RIP or VIP) survey illustrate the utility of this technique in exploring a large area for a possible porphyry system.

DIPOLE-DIPOLE CR-IP LINES

Three dipole-dipole IP lines (0, 1 and 2) were surveyed at North Silver Bell using a dipole spacing of 500 ft. All three lines were planned as nine spreads, but two were expanded to close off anomalous IP responses. The lines were oriented to give a 'spoke-like' pattern of coverage (Figures 5, 6 and 7) that would effectively cover the area of surface projection of the mineralization. Line 0 (Figure 7), at an orientation of N80°W, served as the central line for the CSAMT and magnetic surveys. This orientation was chosen to minimize extremes of crossed topography and to be perpendicular to an inferred major fault. Line 0 is numbered as line 28 on the CSAMT and magnetic surveys. After the initial study in 1993, ZERO personnel returned to the area and conducted a CR-IP survey along line 0 using a dipole spacing of 250 ft. A NanoTEM survey was also conducted along a portion of this line. As this line is close to being east-west oriented, stations along the line are given as the last four digits of UTM eastings (in feet). This could not be done on the other CR-IP lines, so on them conventional electrode numbering is given.

Data for the initial 500-ft dipole lines were acquired with a Zonge GDP-16 three-channel receiver. Data were acquired in a reference complex-resistivity mode with transmission of three fundamental frequencies, 0.125, 1.0 and 8.0 hertz. Standard IP parameters included phase at 0.125 hertz, three-point decoupled phase from the harmonics obtained from 0.125 hertz, and resistivities calculated from 0.125 hertz magnitudes.

Resistivity and phase data from the survey were modeled using a proprietary 2-D smooth-model inversion program. Data in pseudo-section format for each of the lines are displayed on plots (Figures 11-16) that include modeled sections, calculated data and observed data for both resistivity and phase. The calculated data are obtained from the smooth-model inversions and allow a comparison with the observed data to determine the fit of the model. The smooth models permit assigning approximate depths to sources of anomalous response. These depths should be used with caution, as they are dependent on numerous factors including average resistivities, 'off-

line' effects, layering changes, etc. Generally, however, there have been remarkable correlations of smooth-model results with drilling in many different environments. Schematic cross sections of simplified geology and position of the chalcocite enrichment are given for each of the three lines. The geologic sections have a 2.5:1 vertical to horizontal exaggeration.

The lowest resistivities on all three lines can be approximately correlated with the quartz monzonite porphyry or areas of mixed quartz monzonite porphyry and dacite porphyry. There is also a coincidence of lower resistivities with phyllic alteration. Some of the highest IP responses, particularly ones with a shallow component, can also be correlated with the phyllic alteration zones. Examples include stations 7-9 on line 0, stations 9-11 on line 1, and stations 1-2 and 6-9 on line 2. Deeper IP responses as shown beneath stations 3-5 on line 0, stations 0-4 on line 1 and possibly stations 5-7 on line 2 are related to primary mixed sulfide mineralization beneath the chalcocite enrichment zones. Some of the deeper IP response also appears to be 'off-line' effects from highly pyritic phyllic zones. This may be the explanation for the modeled tabular high IP on line 1 at stations 0-5.

One would not expect very high IP responses in the potassic core zones containing primary mineralization of chalcopyrite and pyrite, as estimated total sulfides in this zone are only 2% by volume at most. Phyllic zones, however, can contain 5-7% by volume total sulfides (mainly pyrite). Measurements made on core from within the potassic hypogene zone average only 20-30 mr and not 50-70 mr, such as seen on the modeled deeper anomalies. Relatively high phase values (>50 mr) are obtained from the core measurements of phyllically altered material with high pyrite contents. For these reasons, it is likely that almost all of the higher IP responses on the lines equate to phyllic zones. Assignment of portions of the various IP lines to different alteration types is based solely on the surface alteration map. In the subsurface these contacts may be much different.

More detailed examination of the smooth-modeled resistivities from the three lines reveals some weakly suggestive correlation with leached cap and underlying enrichment. From IP work over other supergene-enriched porphyries, there can be correlation of slightly higher resistivities and essentially little IP response (5-10 mr) to leached cap. This correlation is more apparent where there is an underlying transition into lower resistivities and gradually to dramatically increased phases representing the chalcocite zone and underlying primary mineralization. These relationships are not very distinct over the North Silver Bell deposit, possibly due to the thinness, irregularities and lower-grade nature of the chalcocite zone at this deposit. As the chalcocite blanket is fairly shallow and only 100 ft thick on average, it may be that the larger dipole spacing of 500 ft is not resolving the layer very well. This possibility was investigated in 1996 by conducting a CR-IP line over line 0 utilizing 250-ft dipoles.

COMPARISON OF RESPONSE FROM DIFFERENT DIPOLE SPACINGS ON CR-IP LINE 0

Immediately apparent in the IP response from the 250-ft dipole coverage (Figures 17 and 18) is the absence of the deeper IP anomaly on the western portion of the line as seen with the 500-ft dipole coverage (Figures 11 and 12). Figure 19 is a comparison plot of the coverage from the two different dipole lengths. The modeled shape of the IP anomaly on the eastern portion of the line is fairly irregular for both dipole sizes. The magnitude of the anomalous eastern IP response is similar with both dipole sizes. On the western side of the line, from 2550 to 3550, a strong IP anomaly at depth in the 500-ft coverage is only being weakly sensed with the deepest readings on the 250-ft dipole coverage.

With respect to the known mineralization, the modeled IP response from the smaller dipoles better resolves the thickness of the leached or oxidized cap and the depth to the top of the

chalcocite zone. From 1 to 5 (1550 to 3550) the modeled very low near-surface phases define a layer 100 to 150 ft thick that is equivalent to the leached cap in this area. It is interesting that on the west end of the 250-ft coverage there is a near-surface increase in IP response between –1 and 1 (550 to 1550) that partly coincides with a small increase at the near surface in the 500-ft coverage. It is suggested that the edge of the chalcocite and pyrite zone occurs near here and it is not underlain by significant primary mineralization.

The modeled resistivities for the 250-ft coverage give a sharper depiction of the near surface. At least for a portion of the area interpreted as leached cap on the basis of the modeled IP response, there is a higher-resistivity layer overlying lower resistivities. The higher-resistivity surface layer is shown to be laterally continuous over 2500 ft for the 250-ft modeled data versus 1500 ft for the 500-ft data. The general shape of the modeled resistivities for both dipole sizes are similar except in one area. Between 3800 and 4550 on the 250-ft model there is an extremely low resistivity zone at depth that could represent a major structure or mineralized zone. There is nothing comparable to it on the model of the 500-ft coverage. The low zone in the 250-ft data coincides with anomalous modeled IP responses. This illustrates the different resolving power with changes in the dipole length.

The contrast in responses with different dipole sizes illustrates the need to fit the dipole size to the objectives of a survey. If a large area is to be covered and it is desired to define the limits laterally and at depth of an extensive sulfide system, then a larger dipole size is preferable. If, however, resolution of lateral or vertical interfaces (layers) is desired, a smaller dipole size is desirable. One strategy is to initially conduct a survey with a larger dipole size and then use a smaller dipole size to further define anomalous features.

RECONNAISSANCE (VECTOR) IP

A reconnaissance or vector IP (RIP or VIP) survey was conducted in the North Silver Bell area to assess the utility of this technique in defining a porphyry system within a district-wide context and how the actual response correlates with that obtained from dipole-dipole measurements. The survey followed the general arrangement as was pioneered by Kennecott. A northeast-trending transmitting dipole approximately 5200 ft in length was located 12,000 ft north-northwest of the center of the deposit area. Measurements were made with two orthogonally oriented potential dipoles (Ex and Ey) at 38 stations distributed throughout the area (Figures 6, 20 and 21). Readings were clustered around the North Silver Bell deposit to help define the edges of the system more accurately.

The measurements were made in the non-reference complex-resistivity mode at a fundamental frequency of 0.125 hertz. This allowed for calculation of a three-point decoupled phase from the harmonic frequencies of 0.125 hertz. The potential dipoles were oriented at north-south and east-west, at 45° to the transmitting dipole, to maximize signal for both components and not just one as is done when the dipoles are oriented parallel and perpendicular to the transmitting dipole. The measurements on each dipole were resolved into their real (in-phase) and imaginary (out-of-phase) components. A vector sum of the combined real and imaginary components from the two dipoles was calculated and plotted at the site of the measurement. Apparent resistivity values were calculated and posted.

In the west central portion of the surveyed area, apparent resistivities calculated from the vector IP measurements (Figure 20) define the contact between outcrop and alluvium that may also be the trace of the Atlas fault. To the north of this contact higher resistivities project further to the west, mimicking the presence of outcrop north of the North Silver Bell area. Resistivities over the deposit area appear higher than those determined at the near surface from the dipole-dipole measurements. Resistivities from the RIP survey over the deposit are approximately twice the

shallow (n=1 to n=3) resistivities from the dipole-dipole survey. This probably reflects the contribution of the resistive deeper material below the more openly fractured pyritic zones within the phyllic alteration. In the RIP data, however, there is a trough of lower resistivities that coincides with the higher IP responses over the deposit. This relative decrease in resistivities associated with the higher IP response is the same relationship seen in the dipole-dipole data.

A plot of the vector phase values (Figure 21) shows a strong single point anomaly of 55 mr at station 34 in the southeast corner of the surveyed area. According to Foreman (1994), this strong response is reflecting carbonate replacement sulfides on the edge of the El Tiro system. A moderate strength anomaly (20-35 mr) reflecting the North Silver Bell mineralization occurs to the north of station 34 and is defined by readings at eight stations. The area outlined by the eight stations is approximately 6000 ft by 4500 ft and coincides with the extent of sulfide mineralization defined by the dipole-dipole lines. The northern extent of the RIP anomaly is defined by station 29 with a response of 20 mr which is very close to station –2 on CR-IP line 1, the northern extent of the strong IP response. In an east-west sense, the RIP anomaly is in the same approximate location and of the same width as the modeled IP anomaly on CR-IP line 0. Whereas the anomalous IP response in the CR-IP data varies from 40 to 70 mr, the magnitude of the RIP anomaly is approximately half of that strength. This is easily explained by the much greater volume of ground averaged into the RIP measurements as compared to the dipole-dipole measurements.

There are two single-station RIP anomalies that occur away from the known area of mineralization. One of these at station 14 occurs in an area of alluvial fill, possibly along the projection of the Atlas fault. It is suggested that it may represent a down-faulted portion of the Silver Bell mineralization (Foreman, 1994). Another possibility is that it reflects clays in the alluvium or along the trace of the Atlas fault. Without additional RIP data points or additional data, it is impossible to interpret the anomaly. The other single-station anomaly is on the eastern edge of the survey area at station 23. The source of this anomaly is unknown, but the station is located near outcrop and not over alluvium. It may represent a narrow zone of vein mineralization or possibly a fault.

CSAMT RESPONSES

Five lines, spaced 800 ft apart, of CSAMT data were acquired at North Silver Bell (Figures 6 and 7). Survey logistics for each set-up involved measuring four 200-ft electric-field dipoles with one orthogonally oriented horizontal magnetic-field sensor. A six-channel Zonge GDP-32 receiver was used for the field measurements. A transmitter dipole for the survey was located approximately 17,500 ft north-northeast of the center of the survey area (Figure 6). The frequency range of the survey was from 32 hertz to 8192 hertz in binary increments. Transition from the near field to the far field occurred at 128 hertz, so there were essentially six frequencies of data in the far field. The data for each line were smooth modeled with a proprietary 2-D modeling program. Smooth-modeled resistivity pseudo-sections were plotted for all five lines (Figure 22), but do not allow for unequivocal correlation with geology, alteration or mineralization. Most importantly, the data provide plan views of the smooth-modeled resistivities taken at depth slices of 200 ft, 400 ft and 600 ft (Figures 23-25). With alteration type boundaries and the area occupied by the North Silver Bell stock plotted on the plan views, certain correlations are readily observed.

On the 200 ft and 400 ft depth levels, the areas of lowest resistivities are within the eastern phyllic alteration zone. The western phyllic zone is resistive and may be due to alteration being weak and more disseminated in character with a lot less fracturing and vein control. Graybeal (1982) shows no phyllic alteration on the west side of North Silver Bell and only a minimal

amount on the east side. On Piekenbrock's map (1983), only the weaker types of phyllic alteration occur as a thin band on the southwest side of the North Silver Bell stock, whereas the eastern and northern sides have the strongest phyllic alteration in a fairly wide strip. In porphyry systems, the phyllic zone has the most intense fracturing and strongest pyrite mineralization and sericitic alteration. These characteristics make the zone more conductive. In the potassic zone, there is often silicification, more dissemination of sulfides than as veinlets and lower volumes of total sulfides and clays. These factors should result in higher resistivities within the potassic zone as compared to the phyllic zone. Likewise, the propylitic zone is not as heavily fractured and has much lower total sulfides than the phyllic zone, so it should have higher resistivities associated with it as compared to the phyllic zone. At depth, the 600-ft level, the area of lower resistivities is significantly diminished and the resistivities are not as low as they are at the higher levels. This is probably due to the tighter nature of the fracturing and narrowing of the phyllic alteration developed in the contact zone of the quartz monzonite stock and the dacite porphyry.

CSAMT SMOOTH-MODEL RESISTIVITY FOR LINE 28 COMPARED TO CR-IP SMOOTH-MODEL RESISTIVITY AND NANOTEM SMOOTH-MODEL RESISTIVITY

The smooth model resistivity section for CSAMT line 28 (CR-IP line 0) in the area of the chalcocite enrichment zone has a shallow higher-resistivity response that equates in part to the leached cap above the mineralization (Figure 26). The higher resistivities equate in modeled thickness with the known thicknesses of the leached cap, but the lateral extent of the high resistivity layer is not as extensive to the west as the leached cap and underlying enrichment is known to be. In this western part of the leached cap and underlying enrichment, it is possible that some alluvial cover exists, as this area is below the ridge where the leached cap is exposed. The geologic section also shows the chalcocite zone as thicker and the top of it as shallower than it is to the east beneath the ridge. These factors may help explain why the western area has lower resistivities rather than the higher-resistivity layer that defines the leached cap along the ridge.

An additional electromagnetic technique, NanoTEM, was utilized on line 28 to sense the chalcocite enrichment zone and overlying leached cap. NanoTEM is a transient EM technique that determines resistivities by modeling the decay curve of an induced vertical magnetic field. It is similar to other time-domain loop EM methods, but is able to gather very shallow information as a result of very quick turn-off times and smaller loop sizes. In Chile and other parts of the world where it is difficult to establish good ground contact, TEM methods have been suggested or tested over chalcocite mineralization. Where there is significant enrichment with lots of fracture control, one would expect lower resistivities that could be easily detected with TEM.

The smooth model of the trial NanoTEM line is given above the smooth model of the CSAMT line (Figure 26). The vertical scale on the smooth model of the NanoTEM data is exaggerated with respect to the horizontal scale. The leached cap is readily identified as the high-resistivity layer beneath the thin lower-resistivity surface layer. The modeled resistivities are higher on the NanoTEM line as compared to the CSAMT smooth model, but the thickness and lateral extent of the layer is very similar in both sets of modeled data. On the NanoTEM smooth model, the high-resistivity layer extends slightly further to the east. Beneath the high-resistivity layer in the NanoTEM smooth model, there is a lower-resistivity response that is irregular in aspect. This lower-resistivity zone's upper contact is much more sharply defined in the NanoTEM smooth model than it is in the CSAMT smooth model. There appear to be zones with much more conductivity (lower resistivities), particularly between 3289 and 3944. Whereas this more conductive zone is not as noticeable on the CSAMT smooth model, it could possibly be a small bull's eye feature centered beneath 3800. It is questioned whether this might represent increased

sulfides and enrichment or possibly a fault or fractured zone. Like the CSAMT, the NanoTEM smooth model shows lower resistivities at the surface to the west of the ridge.

Comparing the smooth model resistivity of the 250-ft dipole-dipole data to the CSAMT and the NanoTEM demonstrates good agreement amongst the three techniques in depicting the resistivity layering and environment. The higher-resistivity layer representing the leached cap along the ridge is not as continuous or as pronounced in the dipole-dipole data as compared with the other two techniques. Where layer breaks occur in the smooth model of the dipole data, there are hints of breaks in both the NanoTEM and CSAMT modeled data. Like the NanoTEM model, the higher-resistivity layer in the smooth model of the dipole data extends further to the east then it does in the CSAMT model. Like both the CSAMT and NanoTEM smooth models, the modeled dipole resistivities are low at the surface to the west of the base of the ridge. This similar response in all three techniques suggests that the lower resistivities are real and the expected higher-resistivity response of leached cap does not occur here. It may be that the mixed geology with alternating dacite porphyry and quartz monzonite porphyry is giving a lower-resistivity response. The higher-resistivity response of the leached cap along the ridge occurs in an area that is dominantly dacite porphyry with a few intruded dikes of quartz monzonite porphyry.

COMPLEX RESISTIVITY (CR) MEASUREMENTS

GENERAL BACKGROUND AND DESCRIPTION

As mentioned previously, dipole-dipole IP measurements at North Silver Bell were taken in the reference CR mode. This technique was developed in the early 1970's as a possible means of discriminating the types of sources generating IP anomalies. More specifically, it was hoped that there might be a way to differentiate the IP responses of the various sulfide minerals, particularly pyrite and chalcopyrite. The CR method utilizes Fast Fourier Transforms (FFT's) to obtain the odd harmonic frequencies contained within one transmitted fundamental frequency. Essentially, six harmonic frequencies from the first through the eleventh are obtained for each fundamental frequency.

For the survey at North Silver Bell, three fundamental frequencies were used, 0.125 hertz, 1.0 hertz and 8.0 hertz. With the harmonic frequencies, 18 frequencies of data were obtained for each n-spacing. These data are decoupled to remove the homogeneous earth response and layered-earth coupling. The decoupled spectra are plotted with the real (in-phase) component on the x-axis and the imaginary (out-of-phase) component on the y-axis (Figure 27A). On these spectral plots, frequency increases from right to left and phase increases upwards from the x-axis.

Three general response types (Figure 27B) can be distinguished: 'A', decreasing out-of-phase component with increasing frequency; 'B', consistent out-of-phase component with increasing frequency; and 'C', increasing out-of-phase with increasing frequency. Subtypes of these three responses are 'a', 'b' and 'c'. Numerous laboratory measurements and field tests suggest that pyritic material without other sulfides generally gives an 'A' type spectra. When other sulfides occur mixed with pyrite a transitional type response, often 'B', occurs. A 'C' type response is often associated with propylitic alteration. These types of responses occur irrespective of the overall magnitude of the fundamental IP response, i. e. 2% disseminated pyrite might only have a 30 mr response compared to a 60-70 mr response for 5-6% disseminated pyrite, but both will have an 'A' type response. Other investigators of the spectral IP response maintain that the different response types do not reflect different minerals, but are reflecting differences in grain sizes.

CR RESPONSES AT NORTH SILVER BELL

Laboratory Rock Measurements

To help calibrate the field responses at North Silver Bell, samples were collected from drill core and measured in the laboratory to give IP response at 0.125 hertz, apparent resistivities and spectral plots. Locations of the drill holes from which the samples were taken are shown on Figure 28. Samples of leached cap, chalcocite mineralization, quartz-sericite-pyrite (phyllic alteration) and primary chalcopyrite and pyrite were taken. The plots of the responses (Figure 29) demonstrate a generally flat to slightly bowed 'B' or 'b' type response for the leached cap. The IP response at 0.125 hertz for this type of material is low (6-10 mr). Plots of the spectra for samples from the chalcocite and pyrite zone (Figure 30) are not as unequivocally distinctive as desired. There are some spectra with bowed 'B' type responses, but there are also both 'A' and 'C' types of responses. If anything, the spectra for the chalcocite samples appear transitional between 'A' and 'C' with a tendency to a bowed 'B' response similar to that for the leached cap. Strengths of the IP response for the chalcocite samples vary from 13.5 mr to 63.7 mr.

Spectra of samples from hypogene mineralization (Figure 31) have a mixed character between a slightly bowed 'B' type and an 'A' type. Strength of IP response for the two represented samples is only 18-19 mr. Finally, one spectrum from pyritic phyllically altered material (Figure 31) has a very strong 'A' type response and high IP of 141.8 mr.

Field CR Spectra

For the dipole-dipole lines, the raw and decoupled spectra are plotted at the respective n-spacings in a pseudo-section format (Figures 32-35). Individual spectral plots can also be plotted for each n-spacing, analogous to the plots for rock measurements. Plots of selected n-spacings representative of responses from phyllic zones, chalcocite enrichment and hypogene (Figures 36-38) allow comparison to the spectra from rock measurements. Generally, the spectral types evident in the field measurements correlate with the corresponding alteration and/or mineralization type responses for the rock measurements.

In the field data, chalcocite enrichment zones have a relatively flat 'B' to slight 'A' type response. Phyllic zones with high pyrite contents have a definite 'A' type response and hypogene mixed pyrite and chalcopyrite mineralization has a transitional response from slight 'A' to 'B'. From these spectra, it can be argued that it is not easy to discriminate the chalcocite enrichment response from the hypogene response. Yet, it appears that the phyllic response is distinctive and easily distinguished from the mixed sulfide responses, whether they be chalcocite + pyrite or chalcopyrite + pyrite. In the field data for line 0, spectra on the very ends of the line are 'C' type that is often characteristic of propylitic alteration zones with some disseminated pyrite.

Although not convincingly conclusive, the spectral CR data at North Silver Bell appear to discriminate the pyritic phyllic zones. Whether this is due to monomineralic sulfide content or a difference in grain size and increased fracture versus disseminated mineralization cannot be answered. Regardless of the reason for the distinctive response, it is helpful in determining which portions of a porphyry copper system may contain only strong pyrite mineralization without significant copper sulfides of either primary or supergene origins. A problem in attempting to use CR spectral measurements in a dipole-dipole survey over a porphyry system is that often the strong diagonal effects from shallow, pyritic, phyllic zones overprint the responses from deeper primary sulfides or shallow, thin, laterally discontinuous chalcocite zones. The smooth model can help identify the sources of strongest IP response and remove many of the diagonal effects in the resistivity and phase pseudo-sections, but the modeling cannot remove diagonal effects that may influence the spectral response of specific data points.

REFERENCES

Brant, A. A., 1966, Geophysics in the exploration for Arizona porphyry coppers, in Titley, S. R. and Hicks, C. L., eds., <u>Geology of the Porphyry Copper Deposits; Southwestern North America</u>: Tucson, Az, University of Arizona Press, p. 87-110

Foreman, K. C., 1994, Baseline geophysics over North Silver Bell ore deposit, Pima County, Az: unpublished M.S. Thesis, University of Arizona, Tucson, Az

Graybeal, F. T. , 1982, Geology of the El Tiro Area, in Titley, S. R., ed., <u>Advances in Geology of the Porphyry Copper Deposits; Southwestern North America</u>: Tucson, Az, University of Arizona Press, p. 487-505

Halloff, P. G., 1992, Chapter 2, Electrical: IP and Resistivity with Addendum, in Van Blaricom, R., ed., <u>Practical Geophysics II for the Exploration Geologist</u>: Northwest Mining Assoc., Spokane, Washington, p. 39-176

Kanbergs, K., 1980, Fracturing along the margins of a porphyry copper system, Silver Bell District, Pima County, Az: unpublished M.S. Thesis, University of Arizona, Tucson, Az

Piekenbrock, J. R., 1983, The structural and chemical evolution of phyllic alteration at North Silver Bell, Pima County, Az: unpublished M.S. Thesis, University of Arizona, Tucson, Az

Richard, K., and Courtright, J. H., 1966, Structure and mineralization at Silver Bell, Az, in Titley, S. R. and Hicks, C. L., eds., <u>Geology of the Porphyry Copper Deposits; Southwestern North America</u>: Tucson, Az, University of Arizona Press, p. 157-163

Robinson, R. F., and Cook, A., 1966, The Safford copper deposit, Lone Star mining district, Graham County, Az, in Titley, S. R. and Hicks, C. L., eds., <u>Geology of the Porphyry Copper Deposits; Southwestern North America</u>: Tucson, Az, University of Arizona Press, p. 251-266

Sumner, J. S., 1985, Crustal geology of Arizona as interpreted from magnetic, gravity, and geologic data, in W. J. Hinze et al, eds., <u>The Utility of Regional Gravity and Magnetic Anomaly Maps</u>: Tulsa, Oklahoma, Society of Exploration Geophysicists, p. 164-180

Thoman, M. W. and Zonge, K. L., 1993, Geophysical case history of the North Silver Bell porphyry copper deposit, an oral presentation at the geophysics session of the Northwest Mining Association Annual Meeting in 1993

Titley, S. R., 1982, Geologic setting of porphyry copper deposits, in Titley, S. R., ed., <u>Advances in Geology of the Porphyry Copper Deposits; Southwestern North America</u>: Tucson, Az, University of Arizona Press, p. 37-58

Zonge, K. L., 1972a, In-situ mineral discrimination using a complex resistivity method: Geophysics, v. 38, p. 197

Zonge, K. L., and Wynn, J. C., 1975, Recent advances and applications in complex resistivity measurements: Geophysics, v. 40, p. 851-864

Zonge, K. L., 1992, Chapter 6: Electromagnetics Addendum, in Van Blaricom, R., ed., <u>Practical Geophysics II for the Exploration Geologist</u>: Northwest Mining Assoc., Spokane, Washington, p. 439-536

Note: Numerous general references are not listed. While composing this article, many statements were made based on field geophysical experience and from conversations with K. L. Zonge and other members of ZERO over the years.
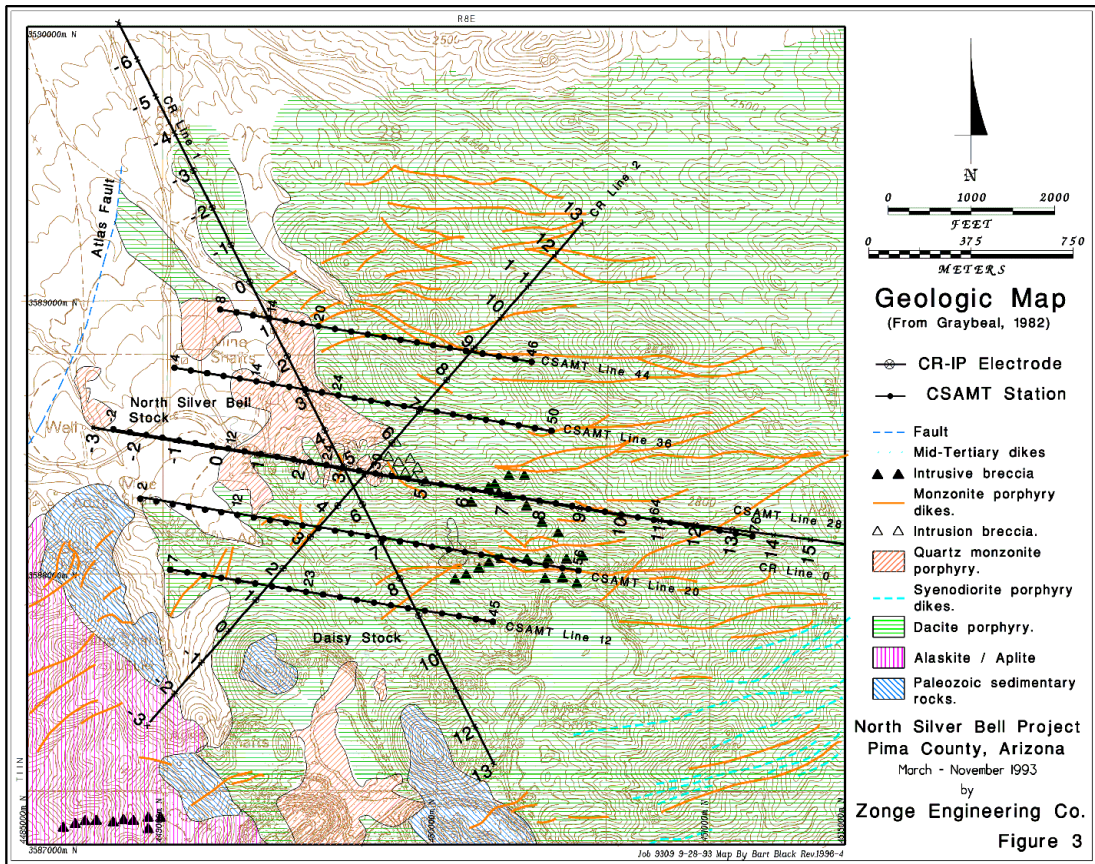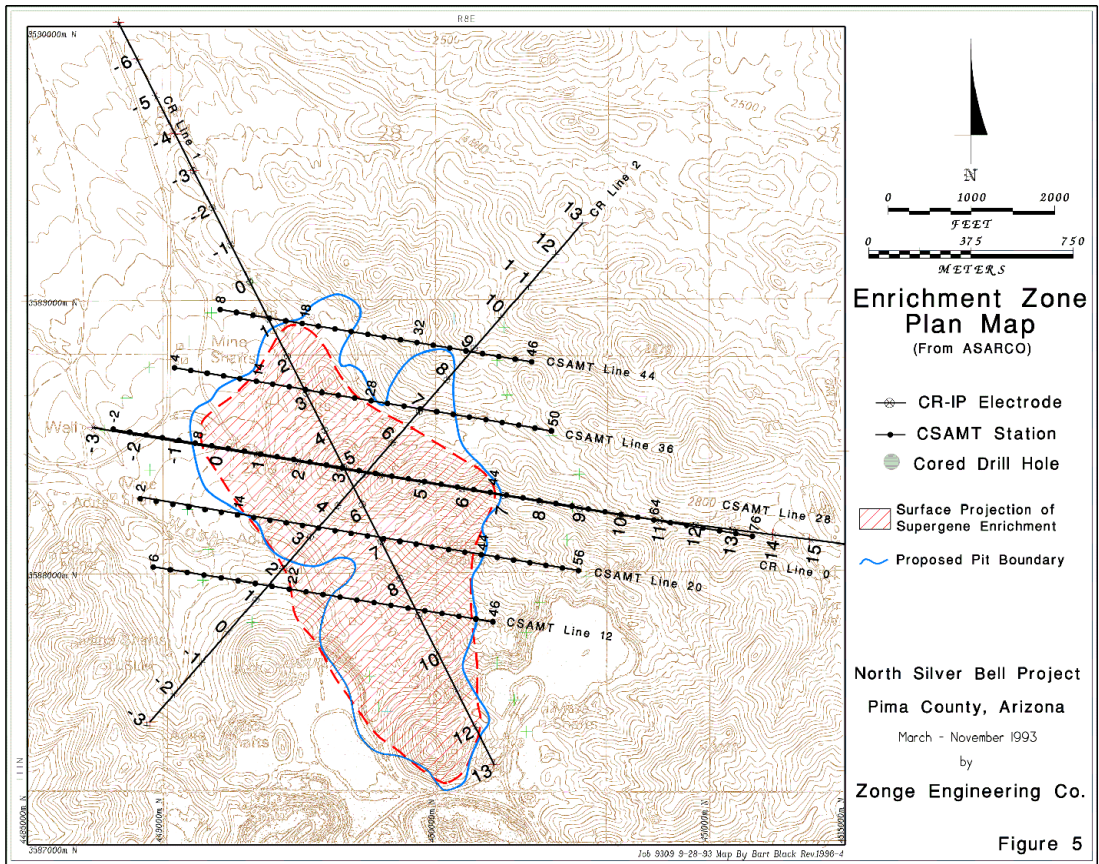
Figure 1 Area Map

Figure 2 General Geologic Map of the Silverbell District from Kranbegs, 1980.

Geologic Map
(From Graybeal, 1982)

⊖ CR-IP Electrode
•— CSAMT Station

--- Fault
·-·-· Mid-Tertiary dikes
▲ ▲ Intrusive breccia
—— Monzonite porphyry dikes.
△ △ Intrusion breccia.
Quartz monzonite porphyry.
--- Syenodiorite porphyry dikes.
Dacite porphyry.
Alaskite / Aplite
Paleozoic sedimentary rocks.

North Silver Bell Project
Pima County, Arizona
March - November 1993
by
Zonge Engineering Co.
Figure 3

Alteration Map
(From Piekenbroch, 1983)

⊖ CR-IP Electrode
•— CSAMT Station

Potassic - Vnlt Assemblages Biot., K-spar-Qtz., Qtz.-Moly.
Propylitic-Diss. Epd., Chl. & Calc.-Rare Epd. Vnlts.

PHYLLIC
Zone 1 Rare Qtz.-Ser.-Py. Vnlts.
Zone 2 Mod. Abundant Qtz.-Ser.-Py. Vnlts.
Zone 3 Strong to Stkwk. Qtz.-Ser.-Py. Vnlts.
∿ Pyrite Boundary

North Silver Bell Project
Pima County, Arizona
March - November 1993
by
Zonge Engineering Co.
Figure 4

Enrichment Zone
Plan Map
(From ASARCO)

⊕— CR-IP Electrode
•— CSAMT Station
🌑 Cored Drill Hole

Surface Projection of
Supergene Enrichment

〜 Proposed Pit Boundary

North Silver Bell Project

Pima County, Arizona

March – November 1993

by

Zonge Engineering Co.

Figure 5

Location Map

Transmitter Locations &
RIP Soundings

⊖ RIP Station Location
— RIP Transmitter
    Location

— CSAMT, CR-IP &
   MAG lines

— CSAMT Transmitter
   Location

North Silver Bell Project

Pima County, Arizona

March - November 1993

by

Zonge Engineering

Grid: UTM Zone 12
Grid Declination 0°18′ West
Base Map USGS Provisional Edition 1989
Silver-Bell West, Arizona
Magnetic North Declination 12°00′

Figure 6

Job 9309 9-9-93 Location Map By Bart Black Rev.1996-4

Location Map

CR-IP
Dipole Spacing 500 ft
CR-IP Rx Electrode Location
CR-IP Tx Electrode Location

MAG Soundings
Station Spacing 100 ft
MAG Station Location

CSAMT Soundings
Dipole Spacing 200 ft
CSAMT Station Location

North Silver Bell Project
Pima County, Arizona
March - November 1993
by
Zonge Engineering Co.

Figure 7

**Figure 8 Residual Aeromagnetic Map of Arizona,
after Sauck and Sumner (1970)**

SILVER BELL
AIRBORNE GEOPHYSICAL SURVEY

COLOR TOTAL MAGNETIC INTENSITY
SHADING NORTHEAST ILLUMINATION

Figure 9

North Silver Bell

Ground Magnetic Survey
Total Intensity Magnetic Field
Reduced to Pole

For Zonge Engineering
Plotted Oct. 1998
by Zonge Engineering

Figure 10

Line 0

Geologic Section of LINE 0

<- N80W Smooth-Model Resistivity (ohm-m) S80E ->

Calculated Apparent Resistivity (ohm-m)

Observed Apparent Resistivity (ohm-m)

Dipole-Dipole data from L0ADC
0.125 hertz, 500 ft dipole data.
ResSmth=1, dpW=0.5, dxW=1, dzW=1

0ft 500ft 1000ft 1500ft 2000ft

Plotted 02/09/99
for Zonge Engineering
Job 9309 by Zonge Eng.

Figure 11

Figure 12

Line 1

Geologic Section of LINE 1

Smooth-Model Resistivity (ohm-m)

<- N 25 W   S 25 E ->

Calculated Apparent Resistivity (ohm-m)

Observed Apparent Resistivity (ohm-m)

Dipole-Dipole data from CRL1
0.125 hertz, 500 ft dipole data.
ResSmth=1, dpW=0.5, dxW=1, dzW=1

0ft   500ft 1000ft 1500ft 2000ft

Plotted 02/09/99
for Zonge Engineering
Job 9309 by Zonge Eng.

Figure 13

Line 1

Figure 14

Line 2

Geologic Section of LINE 2

Smooth-Model Resistivity (ohm-m)

<- S 40 E   N 40 E ->

Calculated Apparent Resistivity (ohm-m)

Observed Apparent Resistivity (ohm-m)

Dipole-Dipole data from CRL2
0.125 hertz, 500 ft dipole data.
ResSmth=1, dpW=0.5, dxW=1, dzW=1

0ft   500ft 1000ft 1500ft 2000ft

Plotted 02/09/99
for Zonge Engineering
Job 9309 by Zonge Eng.

Figure 15

Figure 16

Line 0

Figure 17

Line 0

Geologic Section of LINE 0

Smooth-Model IP (mrad)

Calculated IP Response (mrad)

Decoupled IP Response (mrad)

Dipole-Dipole data from L0BDC
0.125 hertz, 250 ft dipole data.
IPSmth=0.1, dpW=0.5, dxW=1, dzW=1

Plotted 02/09/99
for Zonge Engineering
Job R9604 by Zonge Eng.
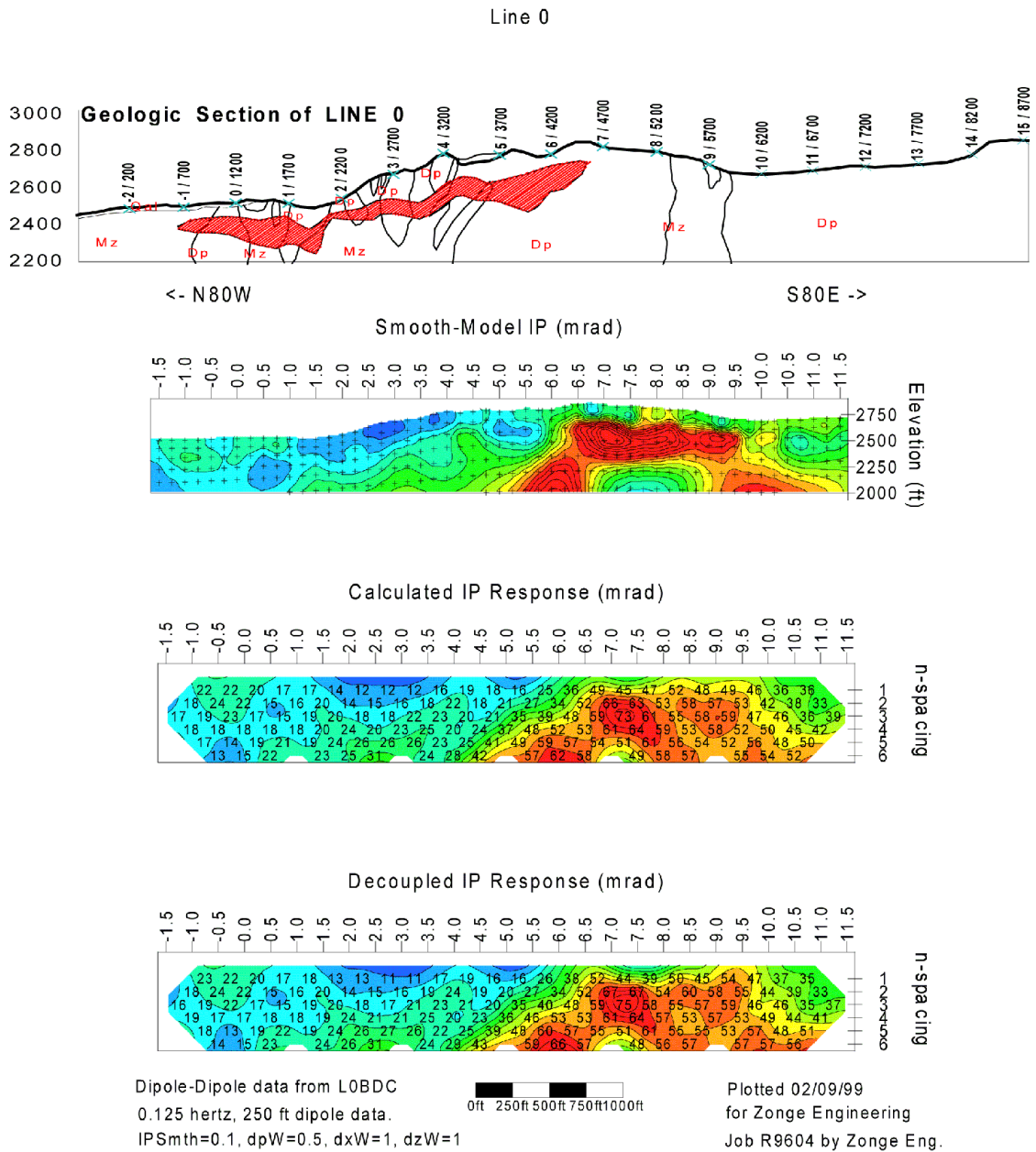
Figure 18

Line 0 CR Survey Smooth-model Sections

Figure 19
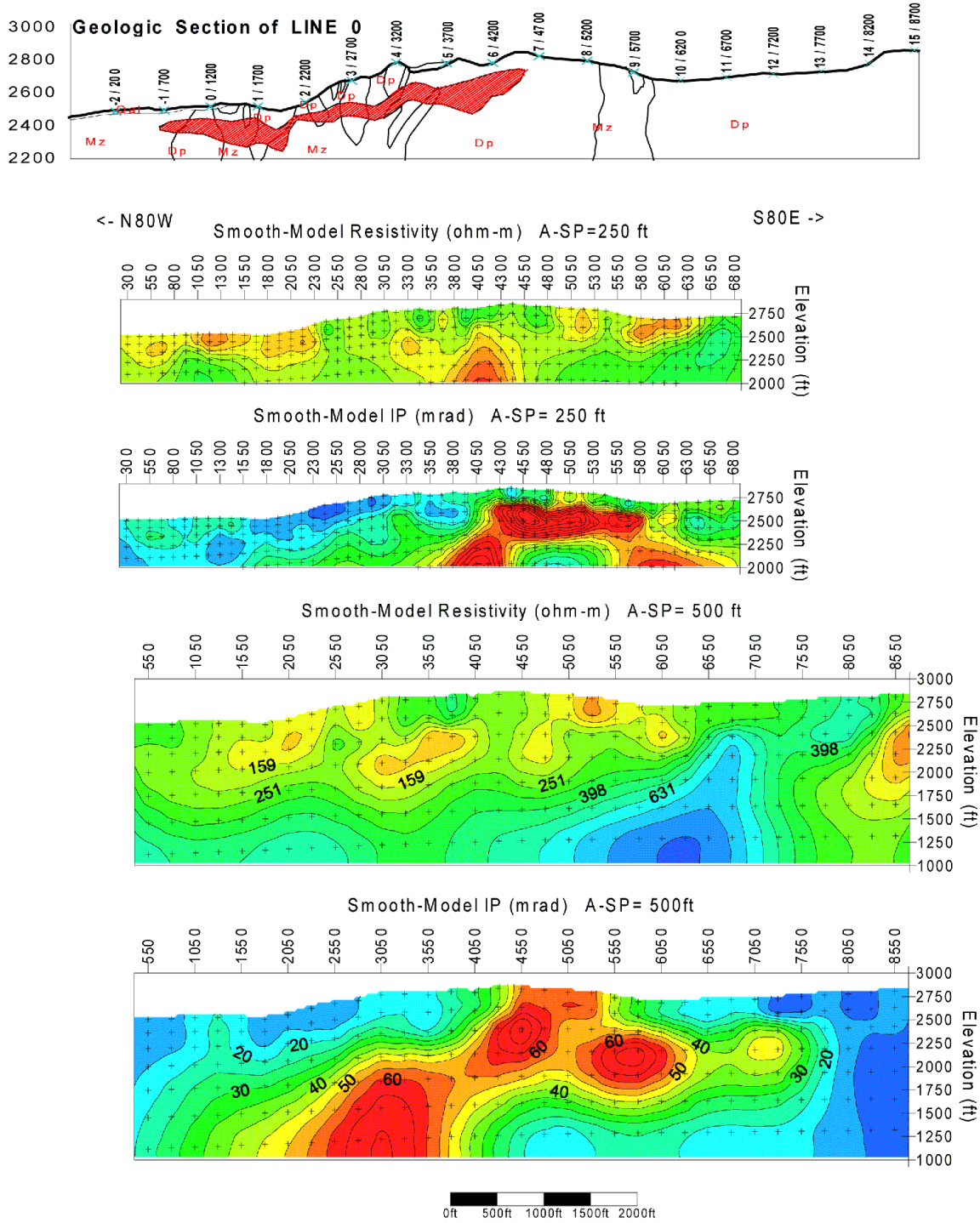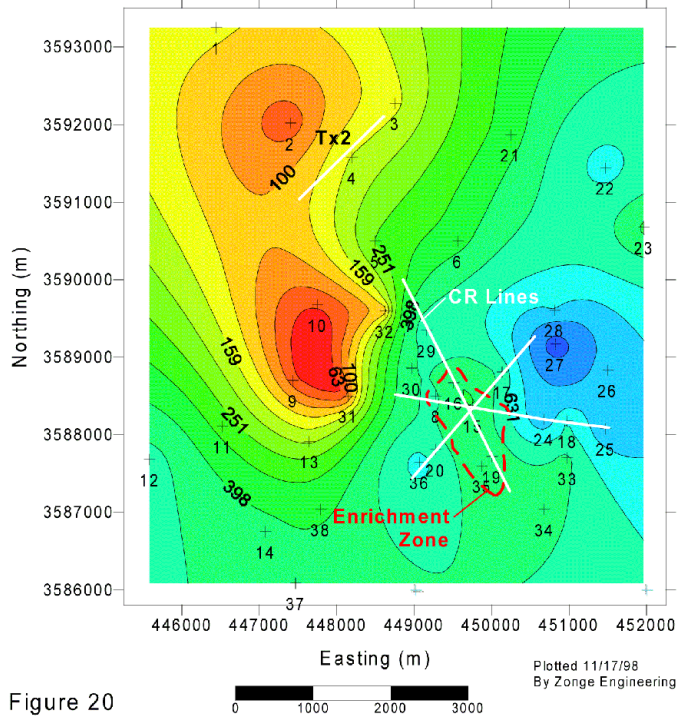
Figure 20

Figure 21

North Silverbell CSAMT Survey
2D Smooth-model Inversion of Resistivity (ohm-m)
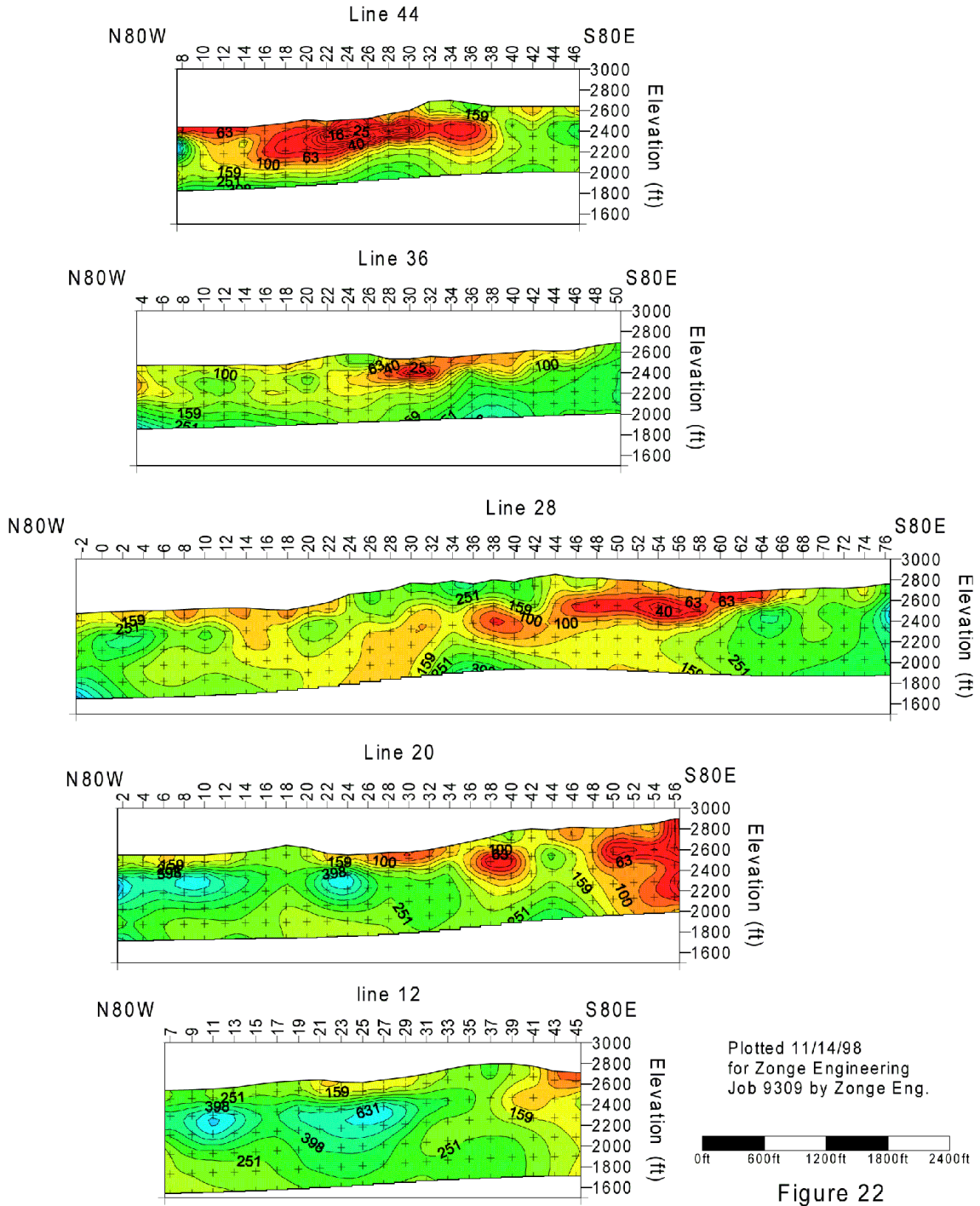
Figure 22

North Silverbell Scalar CSAMT Survey
2D Smooth-Model Inversion Resistivity at 200 foot Depth
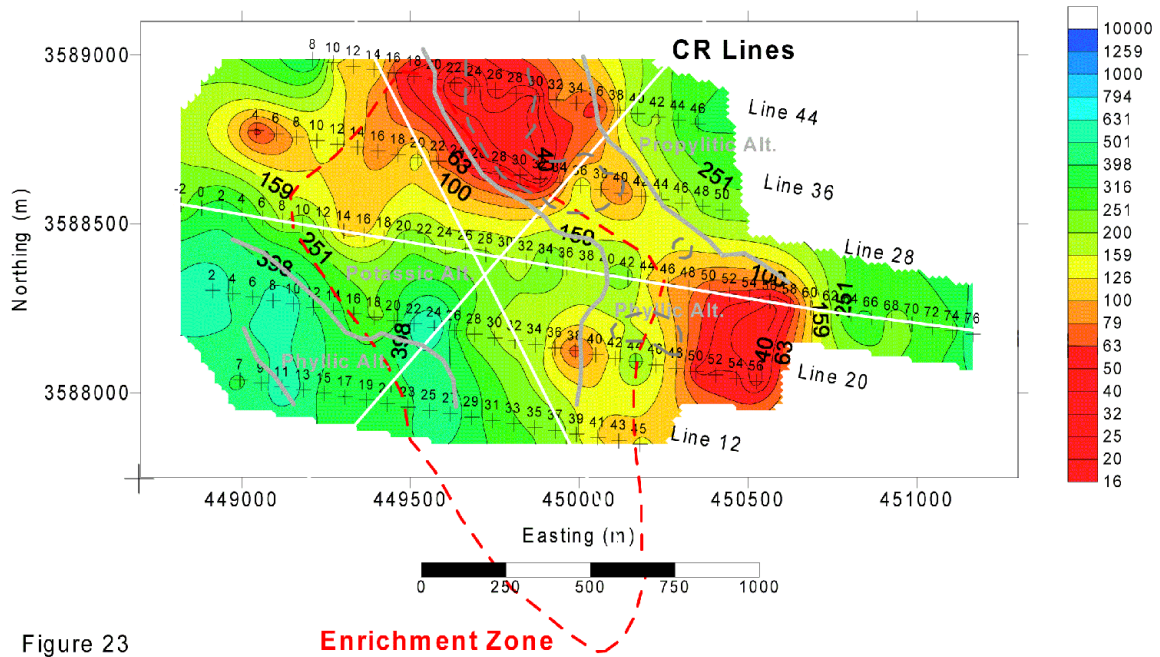
Figure 23

North Silverbell Scalar CSAMT Survey
2D Smooth-Model Inversion Resistivity at 400 foot Depth
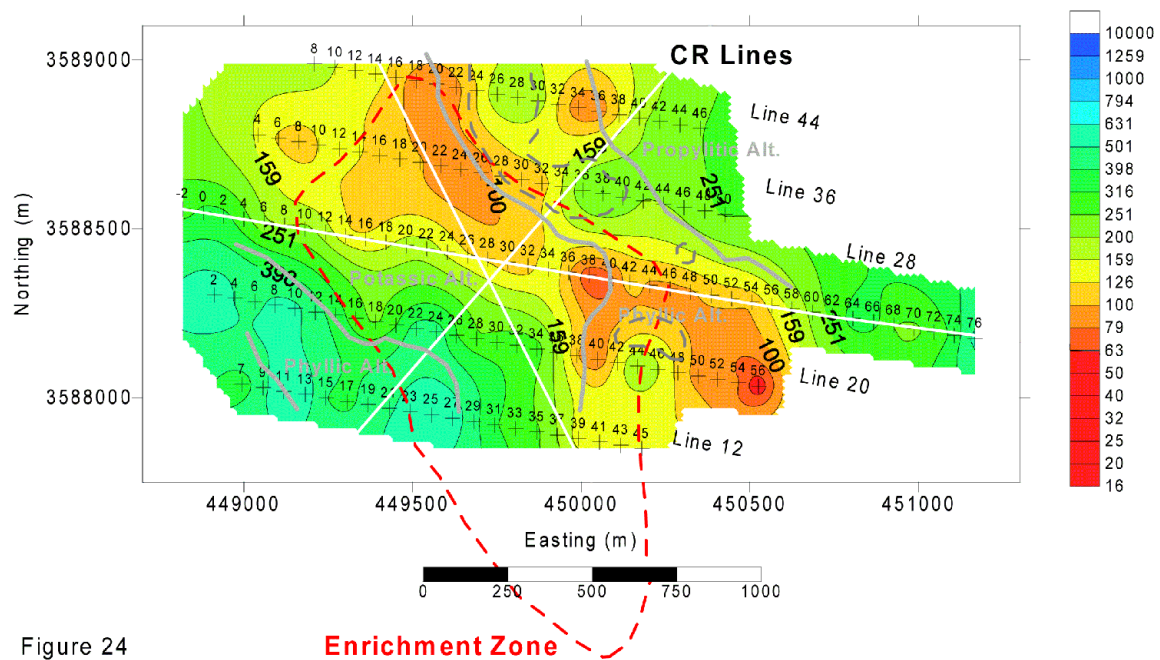
Figure 24

North Silverbell Scalar CSAMT Survey
2D Smooth-Model Inversion Resistivity at 600 foot Depth
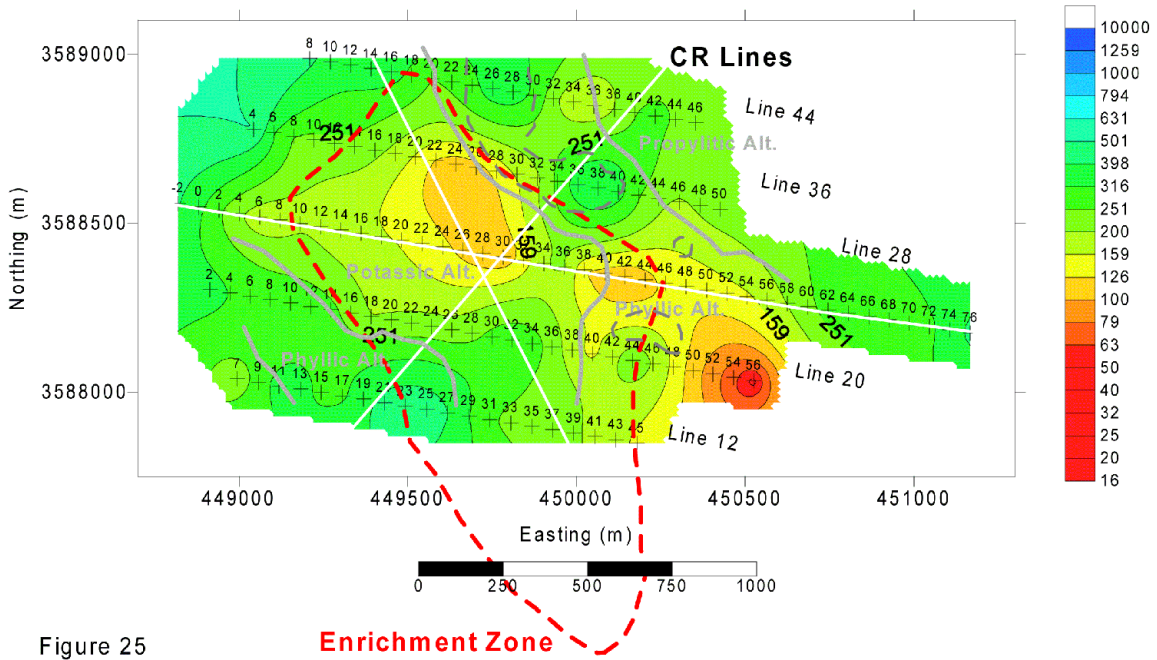
Figure 25
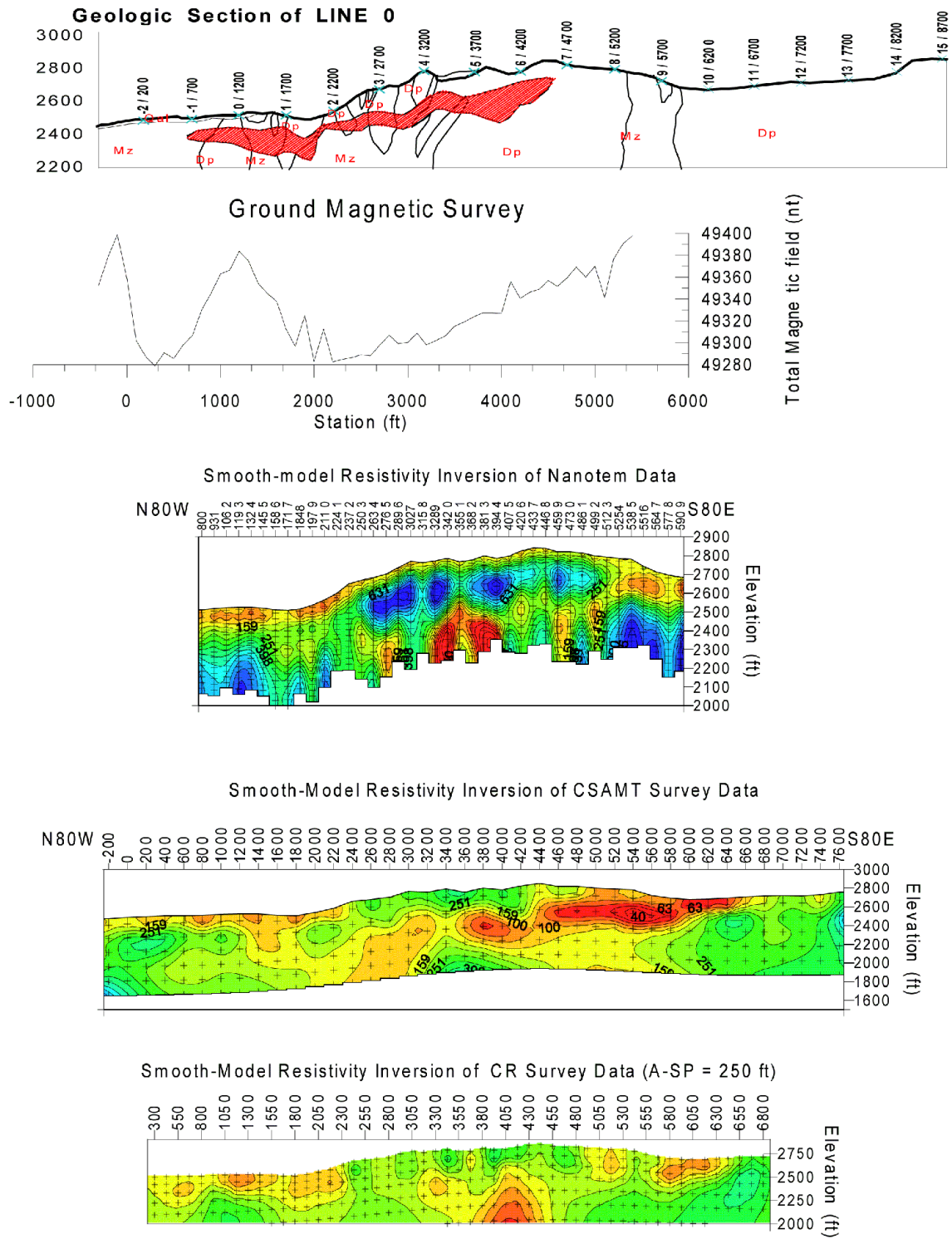
Figure 26
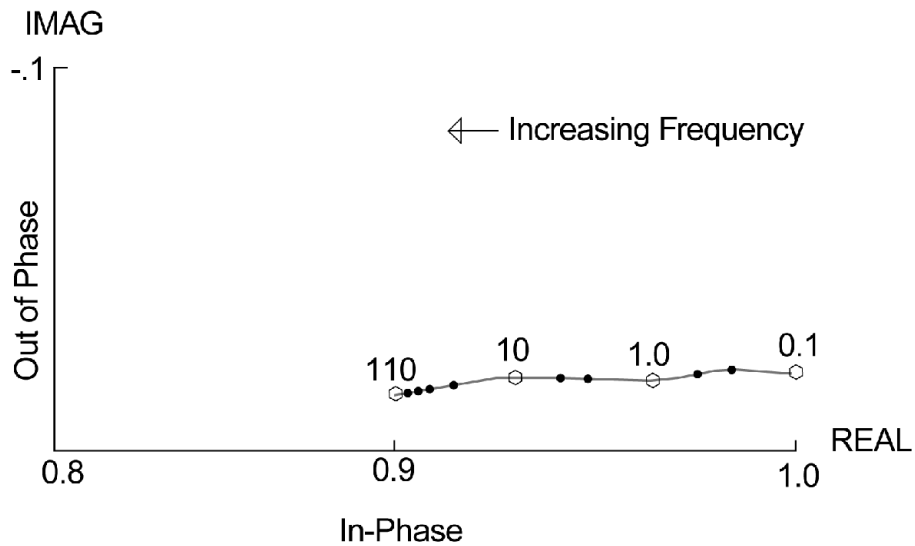
Figure 27A. Classic decoupled CR spectrum for sample containing pyrite and chalcopyrite mineralization. CR spectral data was taken from a 200-foot dipole-dipole survey run over granodiorite porphyry containing pyrite and chalcopyrite mineralization in blebs and veins. Data was decoupled using the same proprietary solution as was used in this study (from Zonge and Wynn, 1975).
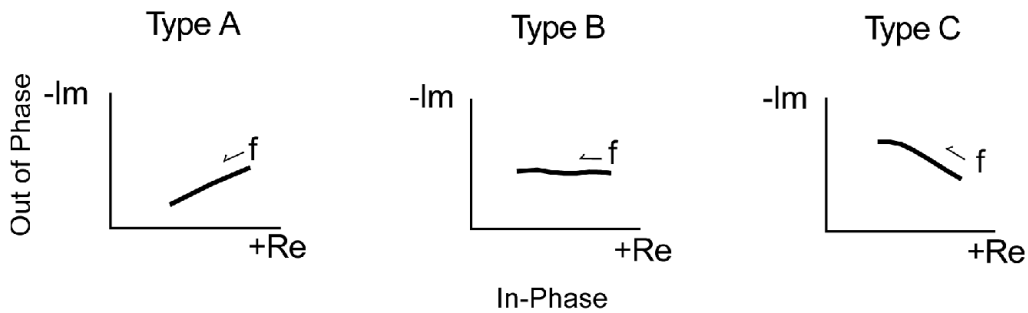
Figure 27B. The ZERO spectral classification scheme.

Type A spectra have a decreasing out-of-phase component (as plotted) with increasing frequency; type c have a corresponding increasing out-of-phase response. These spectral types are further subdivided for descriptive purposes into upper and lower case types as described below.

Type A Slope greater than 20%
      a   20% to 10%
      B   10% to 0%
      b   0% to-10%
      c   -10% to -20%
      C   less than -20%

Enrichment Zone
Plan Map
(From ASARCO)

North Silver Bell Project

Pima County, Arizona

March – November 1993
by
Zonge Engineering Co.
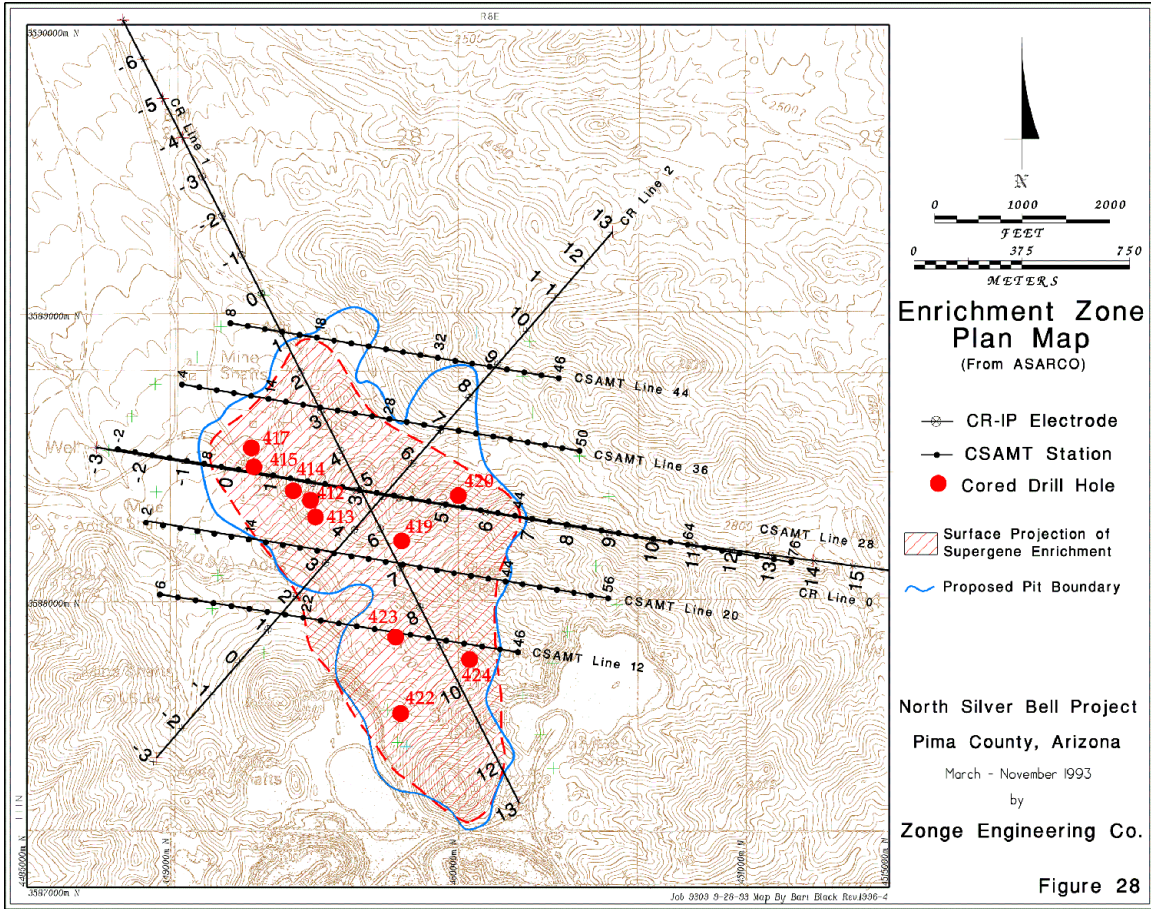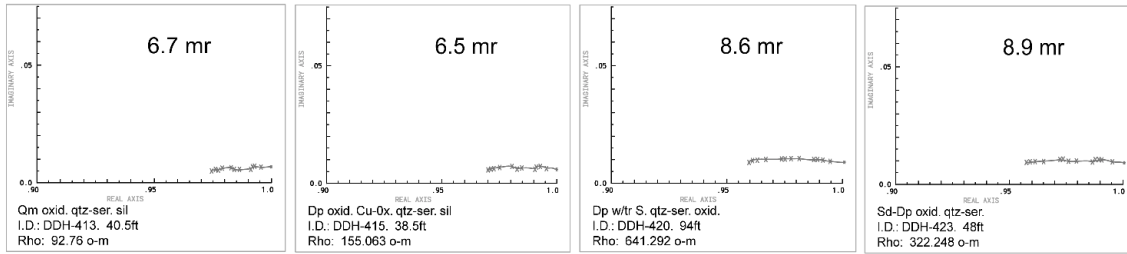
Figure 28

Figure 29 Rock measurements of drill core from oxidized Zone
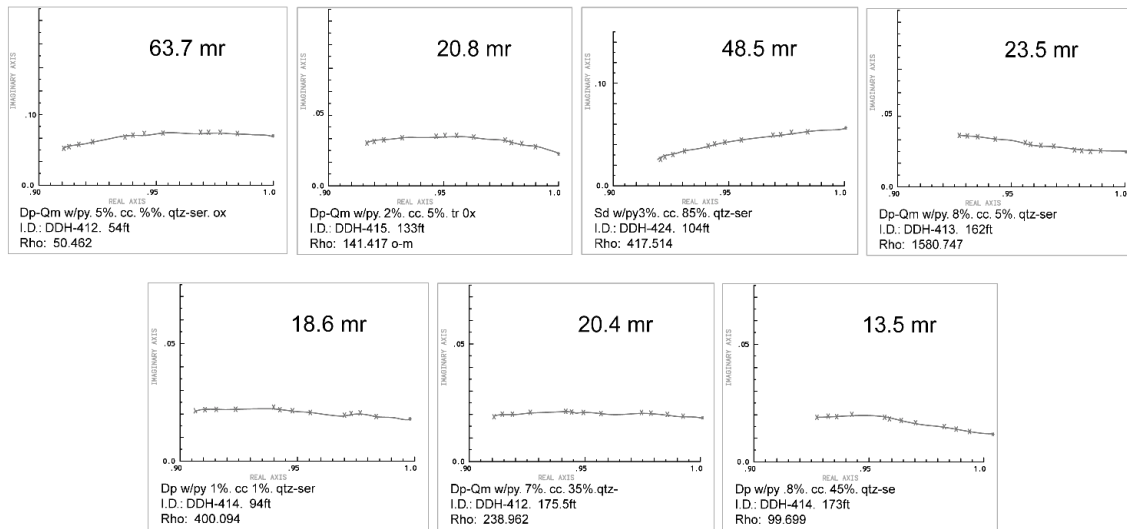
Figure 30 Rock measurements of drill core from Enrichment blanket, Chalcocite and Pyrite
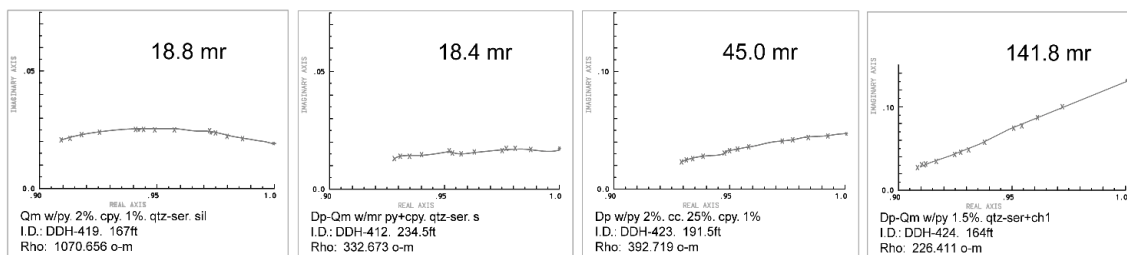
Rock measurements of drill core from Hypogene Zone

Rock measurements of drill core from mixed Sulfides and Just Pyrite

Figure 31

North Silver Bell Project CR Line 0
Spectral Pseudosections   A=500ft

RAW DATA
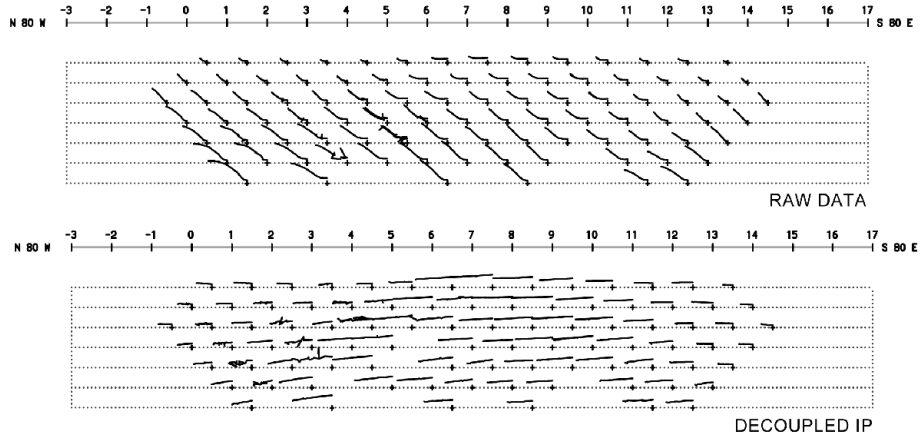
DECOUPLED IP

Figure 32. Raw and Decoupled Spectral Pseudosections for CR Line 0.

North Silver Bell Project CR Line 0
Spectral Pseudosections A=250ft

RAW DATA
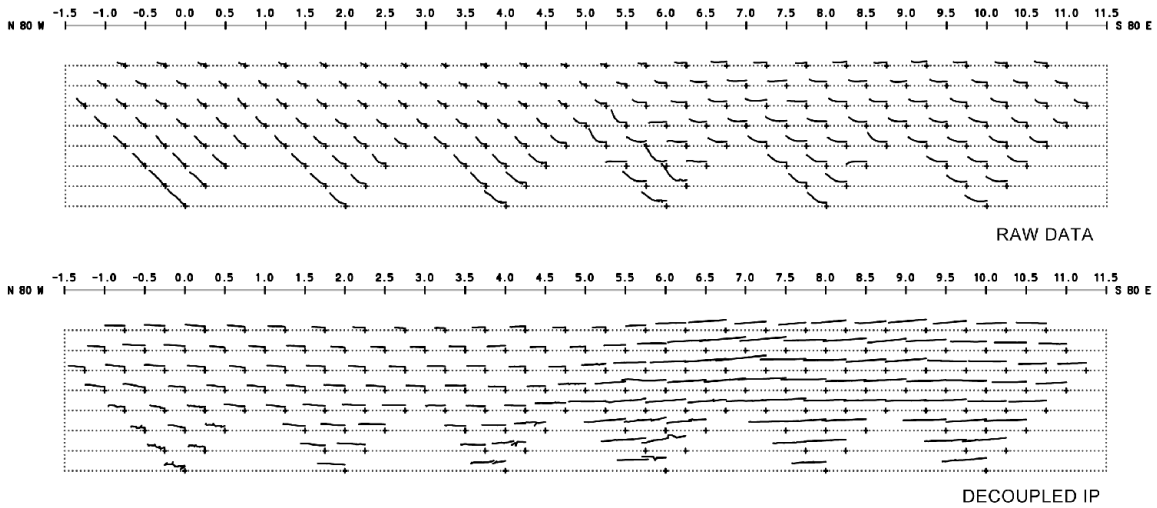
DECOUPLED IP

Figure 33. Raw and Decoupled Spectral Pseudosections for CR Line 0.

North Silver Bell Project CR Line 1
Spectral Pseudosections A=500ft

RAW DATA
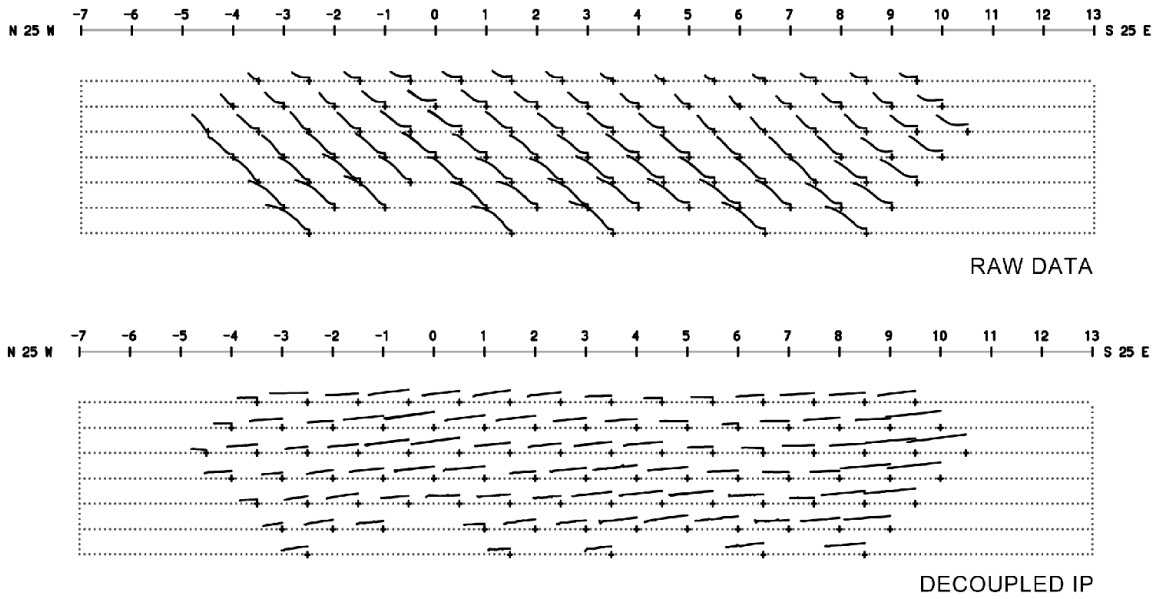
DECOUPLED IP

Figure 34. Raw and Decoupled Spectral Pseudosections for CR Line 1.

North Silver Bell Project CR Line 2
Spectral Pseudosections A=500ft

RAW DATA
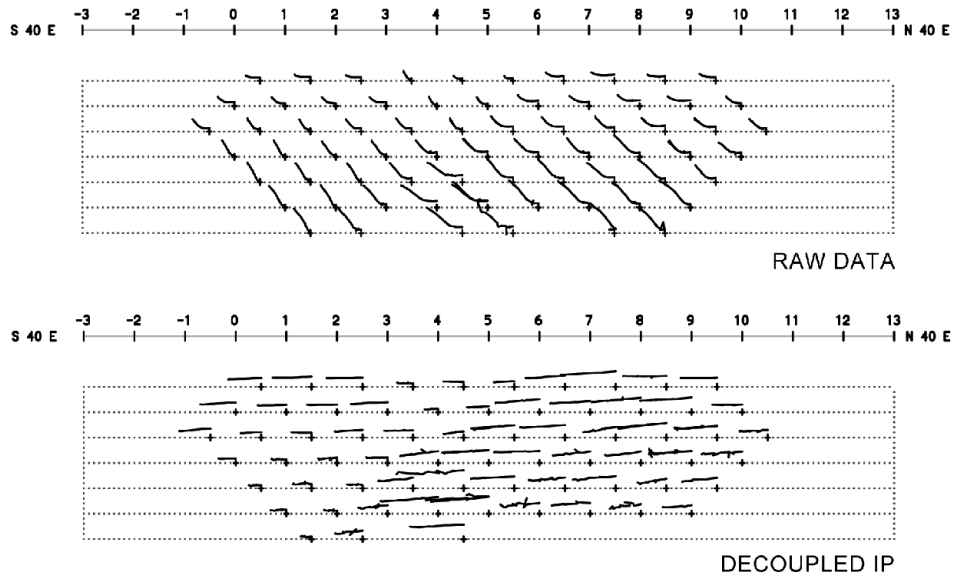
DECOUPLED IP

Figure 35. Raw and Decoupled Spectral Pseudosections for CR Line 2.
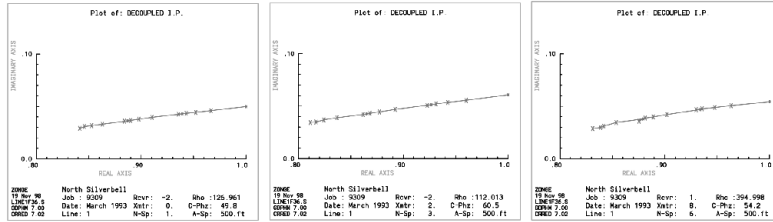
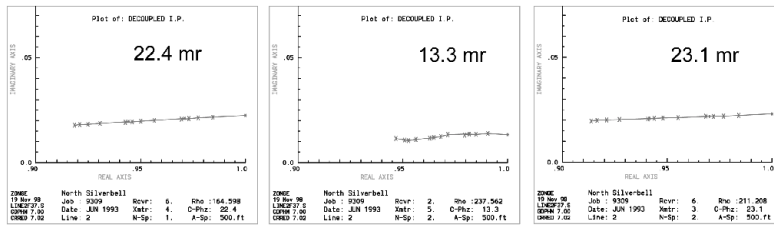Line 1 IP response from NW shallow anomaly and deep response from near line center.
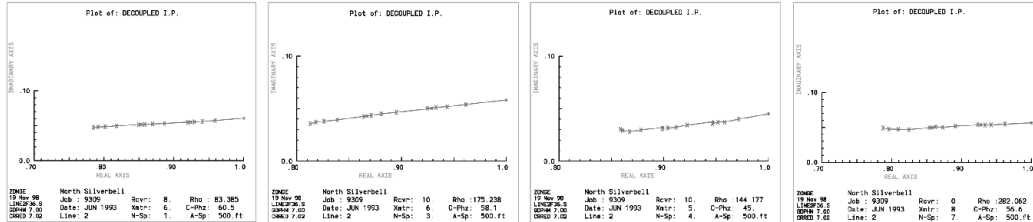
Line 2 IP response from NE shallow anomaly and deep response from line center (Phyllic Alteration)

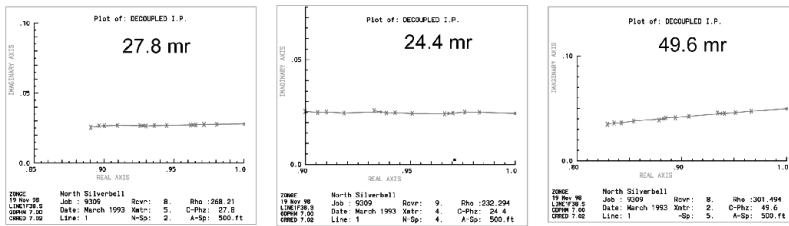Figure 36 Spectral Response of Phyllic Alteration along CR line 1 and 2
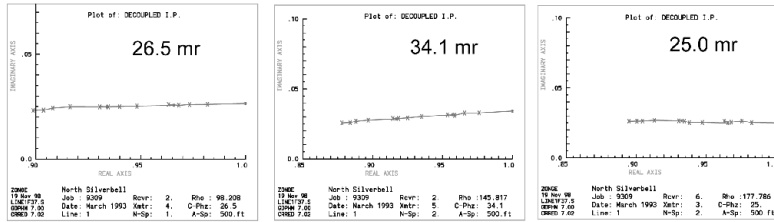
Line 1 IP response over Chalcocite Enrichment zone between stations 2 and 6 at N=1 and N=2.
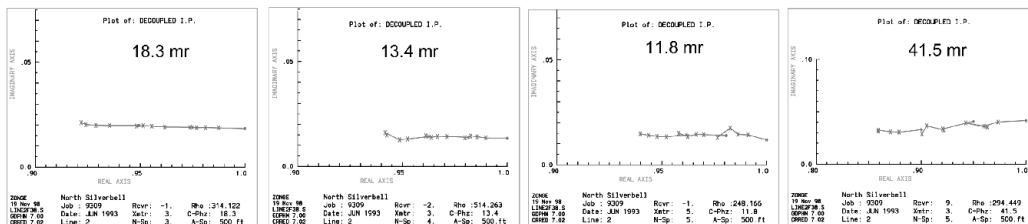

Line 2 IP response over Chalcocite Enrichment zone between stations 2 and 6 at N=1 and N=2.

Figure 37 Spectral Response of Enrichment Blanket along CR line 1 and 2

Line 1 IP response transitional from Enrichment zone into deeper Pyritic/Hypogene zone near line center.

Line 2 IP response transitional from Enrichment zone into deeper Pyritic/Hypogene zone near line center.

Figure 38 Spectral Response of Hypogene Ore System along CR line 1 and 2